ELSEVIER

Isothermal sintering kinetic of 3YTZ and 8YSZ: Cation diffusion

Gustavo Suárez[a,b,*], Nicolás M. Rendtorff[a,b], Alberto N. Scian[a,b], Esteban F. Aglietti[a,b]

[a]*CETMIC, CICPBA-CONICET La Plata, Technological Center of Mineral Resources and Ceramics, Cno Centenario y 506, C.C.49 (B1897ZCA) M.B. Gonnet, Buenos Aires, Argentina*
[b]*Facultad de Ciencias Exactas, Universidad Nacional de La Plata, 47 y 115 La Plata, CP 1900, Argentina*

Abstract

We have studied the sintering kinetic of 3 and 8 mol% of yttria stabilized zirconia under isothermal conditions. Sintering was performed in the temperature range between 1200 and 1450 °C. The sintering kinetic process was followed by measuring density as a function of sintering time. A model was applied to the first stage of densification. Sintering obeys to the grain boundary diffusion mechanism for both materials. It was possible to calculate the activation energy as well as the diffusion coefficients. 887 and 731 kJ mol^{-1} were the activation energies for the initial stage of sintering for 3YTZ and 8YSZ respectively.

Finally the diffusion activation energy was estimated for both materials. The diffusion coefficients were also estimated at 1400 °C in 4.05×10^{-14} and 6.00×10^{-11} cm^2 s^{-1} for tetragonal and cubic zirconia respectively. The obtained results support the observations of a faster densification for 8YSZ.

© 2012 Elsevier Ltd and Techna Group S.r.l. All rights reserved.

Keywords: Zirconia; Kinetic study; Diffusion mechanism; Cation diffusion

1. Introduction

Zirconia materials are widely studied and used in different systems. The tetragonal and cubic phase stabilized with ions such as Ca^{+2}, Y^{+3}, Mg^{+2}, etc. are widely used as structural ceramics and oxygen conductors at high temperatures, including other large number of applications for both zirconia crystalline structures [1–4].

The final properties of these materials can be controlled for by choosing the composition, processing and sintering thermal cycle.

Sintering is the last stage to obtain ceramic materials, and it usually starts at temperatures that are half the melting point of the component. Then, it goes through a sequence of essential phenomena, such as neck formation, pore shrinkage, and grain growth, which results in a solid compact with a suitable microstructure.

In ceramics, the microstructure can define the final properties of the materials, and the sintering process frequently has final unsuitable effects such as grain size growth. For this reason during processing, it is necessary to control the total densification of the material as well as the grain growth, which usually occurs in the last stages of the process.

Fast sintering is an alternative to avoid excessive grain growth during densification [5,6].

Sintering involves the densification and the grain growth. One of the sintering techniques used is the Electric Current Activated Sintering (ECAS) which consists in reaching very high heating rates by the local Joule heating mechanism at grain boundaries; this causes the grain-boundary diffusion (a kinetic effect), and at the same time restricts the grain growth (a thermodynamic effect) [7,8].

Some years ago, a new method called two-step sintering was developed by Chen and Wang [9]. With this method, it is possible to obtain full dense ceramics without the grain

*Corresponding author at: CETMIC, Technological Center of Mineral Resources and Ceramics, Cno Centenario y 506, C.C.49 (B1897ZCA) M.B. Gonnet, Buenos Aires, Argentina.
Tel.: +54 221 4840247; fax: +54 221 4710075.
E-mail addresses: gsuarez@cetmic.unlp.edu.ar (G. Suárez),
Rendtorff@cetmic.unlp.edu.ar (N.M. Rendtorff),
Sciana@cetmic.unlp.edu.ar (A.N. Scian),
eaglietti@cetmic.unlp.edu.ar (E.F. Aglietti).

growth, and the authors explained that this suppression is due to the difference in kinetic between grain boundary diffusion and grain boundary migration. The two-step sintering became a useful technique to obtain very good final properties, and is now widely used in the ceramic field with excellent results [10–13]. Nowadays the two step sintering condition is found by empiric method and not by any thermodynamic study.

It is evident that kinetic study is necessary to enlarge the knowledge in this field, as well as the influence of the substitution content in zirconia. Nevertheless, a complete kinetic study in ceramics is a powerful tool to understand the creep behavior, the effect of oxides deposition in grain boundaries or additives influence in sintering [14,15] within other aspects.

Low temperatures sintering stimulate surface diffusion mechanisms. However, a direct process at high temperature leads to densification mechanisms controlled by others diffusion mechanisms [16].

The kinetic of the sintering process may be followed by measuring the linear shrinkage as a function of time (dilatometry), under non-isothermal conditions, or also by measuring shrinkage or density after holding at constant temperature different times; this method is known as an isothermal sintering kinetic analysis [16–18]. With the use of sintering models, it is possible to determine the sintering mechanism, the activation energy of the process, as well as other physical constants of the system.

In this work, the rapid sintering of dense pieces of tetragonal and cubic zirconia stabilized with 3 and 8 mol% of yttria was studied. No sintering additives were used, and temperature was kept constant between 1200 and 1450 °C. Samples were set at different temperatures with different soaking times. Curves of densities as a function of time between 5 and 180 min were determined. The curves were analyzed using sintering models developed by Kingery and Berg [19].

Diffusion activation energy and sintering parameters of the process were evaluated as well as cation diffusion coefficients.

2. Experimental

2.1. Materials

Powders with 3 mol% (3YTZ) and 8 mol% of Y_2O_3 (8YSZ) stabilizing the zirconia tetragonal and cubic structure respectively (commercially named as YZ01 and Y8Z01, Saint-Gobain, France) were used in this study. The X-ray diffraction analysis by the Garvie-Nicholson relation [20] shows that 24 wt% of monoclinic phase is present in the tetragonal zirconia at room temperature. At 1000 °C the monoclinic phase turns to tetragonal structure. The 8YSZ zirconia powder used presents fully stabilized cubic phase in all the temperature range. The mean particle diameter and the specific surface area given by the manufacturer for both samples are 0.6 μm and 7.0 $m^2 g^{-1}$ for tetragonal zirconia and 0.53 μm and 8.26 $m^2 g^{-1}$, for cubic zirconia.

2.2. Sample preparation

Samples were shaped by slip casting in plaster molds. Zirconia slurry with 80 wt% solid content was prepared. The deflocculant ammonium polyacrylate solution NH_4PA (Dolapix, Zschimmer & Schwartz) was used in an optimum content 0.1 wt% [21]. The pH was adjusted with ammonia solution (25 wt%) at 9.5. Aqueous slips were prepared by deagglomeration of the powder in de-ionized water by ultrasonic treatment.

The powder was added in portions to the suspensions and the pH was manually adjusted to be maintained at a desired value during the additions. Prismatic bars were prepared by slip casting. After drying, small pieces of 10 mm × 10 mm × 5 mm were cut, and used to study the evolution of the sintering process. Green densities of the probes were 4.00 for 3YTZ and 3.47 g/cm³ for 8YSZ, which means 65% and 60% of the theoretical density respectively, assuming 6.059 for 3YTZ and 5.959 g/cm³ for 8YSZ as theoretical density.

2.3. Sintering and characterization of the sintered samples

Dried compacts were sintered at five different temperatures between 1200 °C and 1450 °C during variable periods of time between 5 min and 180 min. The samples were preheated at the temperature of 700 °C for 1 h by placing them in the external part of an alumina tube going outside the furnace lid, with its opposite extreme remaining inside the furnace [22]. Thus, the samples did not suffer thermal shock when exposed to the sintering temperature. After this preheating step, the samples were rapidly placed inside the furnace. The measuring of the initial time was started when samples were placed in the high temperature region of the furnace. The samples were held at the sintering temperature for a desired period of time, then they were immediately transferred to a low temperature region in the furnace and, finally, they were cooled (quenched) at room temperature.

As the largest densification increases occurred during the exposure at high temperature, this sintering procedure can be considered nearly isothermal. The bulk density of sintered probes was determined by Archimedes method in water. Pore size distribution of sintered compacts was measured by Hg porosimetry (Porosimeter 2000, Carlo Erba). The microstructures were observed by scanning electron microscopy (SEM, JEOL JSM 6360LV) on polished sections after thermal etching.

3. Results and discussion

3.1. Densification curves

Densification curves as a function of time are shown in Fig. 1 in the temperature range of 1200–1450 °C for 3YTZ and 8YSZ. It is observed that, with the increase of the sintering temperature, the maximum density achieved at a
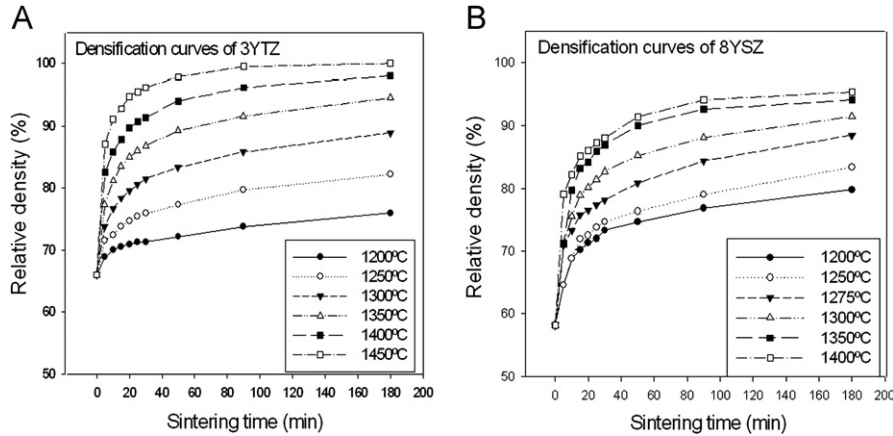
Fig. 1. Densification curves of (A) 3YTZ and (B) 8YSZ at different temperatures and different holding times.

certain temperature is reached at shorter times. Nevertheless in this stage of analysis it is difficult to assume a sintering rate. For this reason, a further analysis with sintering models needs to be realized.

From the direct observation of these curves it can be seen that 8YSZ presents a high initial sintering rate. This assumption is premature because the densifications need to be analyzed deeply.

3.2. Sintering models and activation energy

3.2.1. Sintering mechanism and activation energy

Density as a function of time curves were analyzed by employing the sintering models developed by Kingery and Berg [19], and Coble [17], and widely used by Matsui et al. [23].

The following equation can be developed from the simplest equation of shrinkage for isothermal sintering:

$$\left(\frac{\Delta L}{L_0}\right) = (B'' t)^n \tag{1}$$

where ΔL is the difference between the final length and the initial L_0. B'' is a constant and t is time in seconds.

For small shrinkage [19], it can be assumed the relation expressed as

$$\left(\frac{\Delta L}{L_0}\right) = \frac{1}{3}\left(\frac{\Delta V}{V_0}\right) \tag{2}$$

Replacing Eq. (2) in Eq. (1), the following equation is obtained:

$$\frac{1}{3}\left(\frac{\Delta V}{V_0}\right) = (B'' t)^n \tag{3}$$

Expressing volume as mass–density relation, calculating natural logarithm (ln) in both parts of the equation and adding the constant $1/3$ in the constant B'' we get the following equations:

$$\left(\frac{\Delta V}{V_0}\right) = \left(\frac{d-d_0}{d}\right) = (B' t)^n = B'^n t^n \tag{4}$$

$$\ln\left(\frac{d-d_0}{d}\right) = n\ln(B') + n\ln(t) = \ln(B) + n\ln(t) \tag{5}$$

where d stands for density at time t and green density is d_0. Parameter B'' multiplied by the constant $3^{1/n}$ became another constant named B'. Besides $\ln(B)$ is equal to $n\ln(B')$ and n is given by the order of this process.

Eq. (5) describes, in general, the kinetic of a sintering process given by the variation of density with time at constant temperature.

The n value depends on the sintering mechanism predominant in the process. Both n and B values are obtained by plotting Eq. (5) in Fig. 2 and using experimental data for times lower than 30 min, assuming those times corresponding to the first stage of sintering.

In this case n indicates the sintering mechanism and B is a variable behaving like an activated process following an Arrhenius law which is defined by Eq. (6). B and B_0 are directly related to the sintering kinetic constant k and k_0:

$$B = B_0 \exp\left(\frac{-Q}{RT}\right) \tag{6}$$

$$\ln(B) = \ln(B_0)\frac{-Q}{RT} \tag{7}$$

In this work, for low temperatures the sintering time can be in a wide range keeping the shrinkage up to 4%. For higher temperatures, the sintering time is very short if we strictly consider the initial stage and not many data point can be used.

Analyzing the linearity for times up to 90 min, it is observed in Fig. 2 that the linearity does not change.

The present study is done extending the limits of shrinkage higher than 4% because it is demonstrated that the system behavior represented by the linearity in Fig. 2 cover the study of the initial stage of sintering and part of the intermediate sintering stage.

Straight lines in Fig. 2 show that the experimental values are consistent with those calculated by employing Eq. (5).

In order to distinguish between the possible diffusion mechanisms involved such as evaporation–condensation,
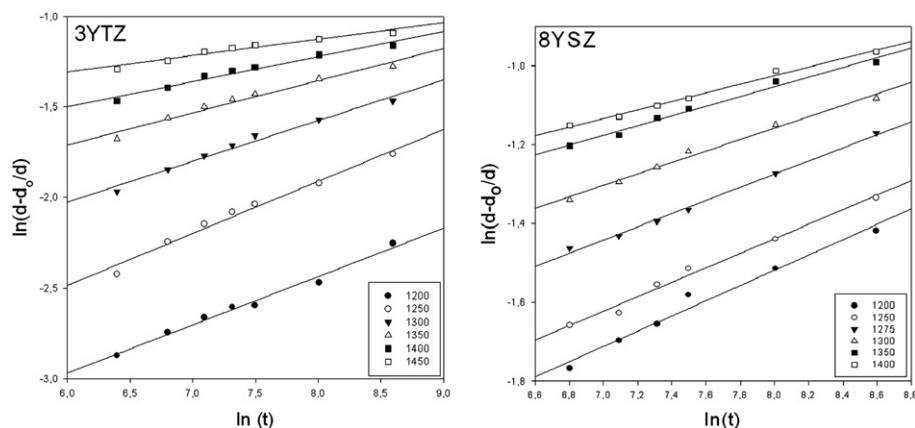
Fig. 2. $Ln(d-d_o/d)$ vs ln t plots show the linear relation between density change and time. The data taken for 3YTZ and 8YSZ compacts sintered at different temperatures during short times.

grain boundary or volume diffusion, a method based on the density variation of the sample as a function of time at different temperatures was used here.

With the experimental data obtained from Eq. 5 and plotted in Fig. 2, the exponent n for 3YTZ and 8YSZ resulted between 0.15 and 0.30. Evaporation–condensation and grain boundary diffusion are mechanisms characterized by the fact that there is no noticeable shrinkage of the sample volume. Kingery and Berg [19] observed that, in the volume diffusion mechanism, the particles join together as evidenced by an increase in the neck area formed between particles that caused an increase in density.

Exponent n was obtained from the slope of the lines at the different temperatures, between 0.20–0.30 for 3YTZ and 0.17–0.25 for 8YSZ, which indicates that the mechanism is the same over the studied temperature range for both materials and belongs to grain boundary diffusion (GBD).

Previous studies reported that, at initial sintering stages for these kinds of materials, the process could also take place according to the grain boundary diffusion mechanism [22,24–26]. This phenomenon was observed for a material sintered at a temperature lower than the effective one for a complete sintering.

The activation energy Q and the pre exponential factor B_0 of the Arrhenius equation can be estimated from the data B obtained at each temperature (Fig. 2) and using Eq. 6.

Fig. 3 shows the Arrhenius plot of the sintering process for 3YTZ and 8YSZ. Linearity was satisfactory. According to this figure, the densification was an activated process with activation energy of 887 kJ/mol for 3YTZ and 731 kJ/mol for 8YSZ.

Activation energy can be considered as a parameter to control the sintering rate: the higher the activation energy; the lower the sintering rate. For similar initial particle size and chemical composition, the difference in activation energy might be attributed to the yttria concentration in both samples.

Zirconia stabilized with 3 mol% of yttria was presented by Matsui et al. [25] with an activation energy of 683 kJ/mol, Wang and Raj [27] estimated in 615 kJ/mol, Chaim [28]
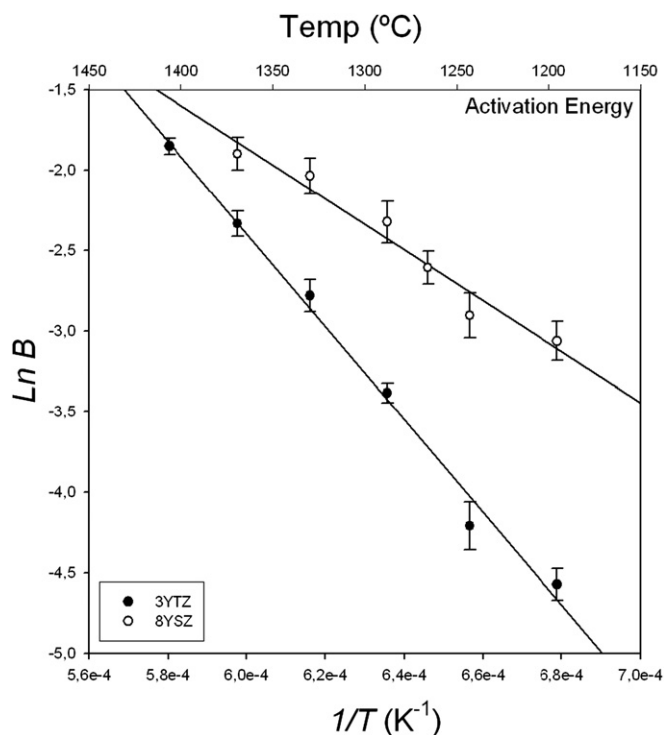

Fig. 3. Arrhenius plot of the sintering process for activation energy calculus.

presented the activation energy of 3YTZ between 460 and 720 kJ/mol. Instead, 8 mol% of yttria stabilizing zirconia was also studied and some activation energies were estimated. Matsui et al. [25] presented 757 kJ/mol. The activation energy can vary from different authors because of the inherent differences between powder characteristics but it is clear that the tendency in this parameter is that 3YTZ presents higher activation energy, hence a lower densification rate at the initial stage of sintering.

3.2.2. Diffusion coefficient

Solid-state sintering takes place in three well defined concurrent stages: neck formation, pore contraction, and

grain growth. Each stage is characterized by a density and a typical microstructure.

At the initial stage, neck formation takes place (contact surface between particles) and no increase in grain size is observed as compared with the initial one.

At the following stage, neck increases to reach an area covering about 1/5 and 1/3 of the particle diameter. This is shown by 3–5% shrinkage and a 65% of theoretical densification.

Factor B' in Eqs. (5) and (6) is presented by Kingery and Berg [19] as follows:

$$\left(\frac{\Delta V}{V_0}\right) = (B')^n t^n = \left(\frac{80\gamma\Omega D_v}{kT}\right)^n t^n \qquad (8)$$

where Eq. (8) is the same as Eq. (3) with B presented in Eq. (9) as follows:

$$B' = \left[\frac{80\gamma\Omega D_{GBD}}{kT}\right] \qquad (9)$$

D_{GBD} is the diffusion coefficient for the grain boundary mechanism estimated above, γ the surface energy (a value of 1000 erg was taken [29]); k the Boltzmann constant; T the absolute temperature and Ω the atomic volume of a vacancy (1.717×10^{-23} cm^3).

Particle shape and initial size ratio are important variables for shrinkage measurements. Similarly, the size distribution effect on sintering rates should be also considered if kinetic parameters would be compared with those of spherical particles of a monomodal distribution. The particle size influence on the diffusion sintering mechanism (global mechanism) suggests that the fine sized particles of the distribution will be the most important ones; it was observed that the size representing the distribution is neither that of the fine sized particles nor of the mean sized ones, therefore the use of a mean size in the calculation will lead to higher diffusion coefficients. It must be also taken into account that the models assume a constant particle size during the sintering process.

Moreover, if at the initial stage, grain growth occurs simultaneously, the diffusion coefficient calculated from shrinkage measurements will be relatively lower than that calculated considering the grain growth taking place at the end of the process.

Finally, neck formed between spherical particles is assumed to have circular geometry in the different sintering models. This fact leads to the calculation of lower coefficients if diffusion of vacancies is the predominant mechanism. The mean particle diameter was considered here the same for both materials ($Dp = 0.5 \mu m$).

From Eq. (9) and using the B values obtained from experimental data for different temperatures, the grain boundary diffusion coefficient (D_{GBD}) was calculated.

The intervals of time used were chosen in order to reach density values lower than 75% of the theoretical one, except for the higher temperature ones 1350–1450 °C where nearly 85% was achieved.

The high mobility of the oxygen ions in yttria stabilizing zirconia together with the high melting point suggests that the cation diffusion will be controlling the diffusion in these materials.

Fig. 4 shows a linear variation of $Ln(D_{GBD})$ with the inverse temperature.

The diffusion coefficient can be presented as an activated process depending on the sintering temperature as follows:

$$Ln(D_{GBD}) = Ln(D_{GBD}^0)\frac{-Q}{RT} \qquad (10)$$

From a ln–ln plot of Eq. (10), it was possible to linearize in Fig. 4 and calculate the activation energy of the diffusion process for both 3YTZ and 8YSZ being 255 and 202 kJmol^{-1} respectively. The values are in concordance with previous results [22].

Then, the diffusion coefficient can be calculated from Eq. (10) as follows:

$$D_{GBD} = D_{GBD}^0\exp\left(\frac{-Q}{RT}\right) \qquad (11)$$

The grain boundary diffusion coefficient for Zr in 3YTZ and 8YSZ was calculated by $D_{GBD} = 87,100 \times e^{-255/RT}$ and $D_{GBD} = 19,953 \times e^{-202/RT}$. Using this expression, the D_{GBD}Zr obtained was 4.05×10^{-14} cm^2 s^{-1} at 1400 °C for 3YTZ and 6.00×10^{-11} cm^2 s^{-1} at 1400 °C for 8YSZ these obtained diffusion coefficients are consistent with the ones reported in literature for similar materials [18,22].

In cation diffusion, higher activation energy involves a lower diffusion rate. For tetragonal and cubic zirconia at 1400 °C, we can observe that tetragonal zirconia presents a
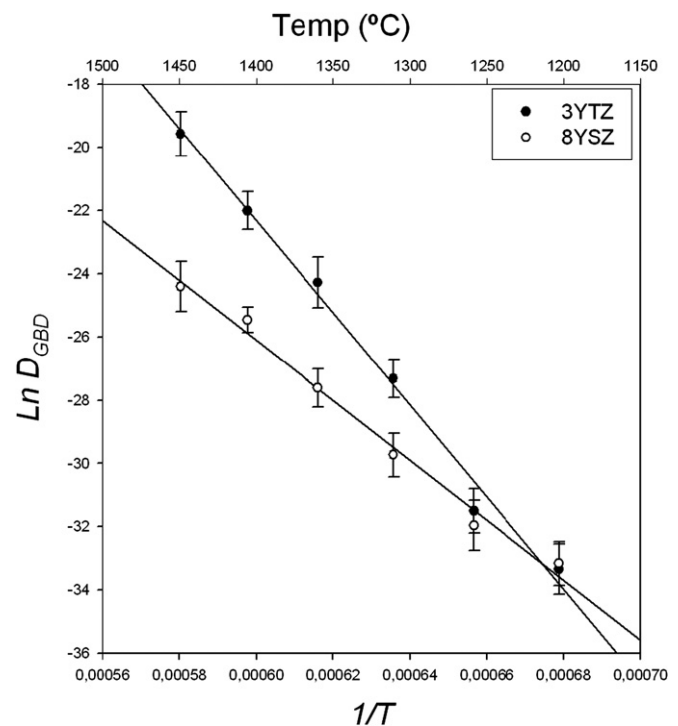

Fig. 4. $Ln\,D_{GBD/Zr}$ (diffusion coefficient) vs. $1/T$ of samples held at different temperatures for a short time.

smaller diffusion coefficient which is in concordance with the higher activation energy.

There are many factors affecting the calculation of diffusion coefficients. Matsui et al. [23] also describe the effect of the surface area in activation energy and they reported that higher surface area affect the activation energy of sintering by decreasing it. This is the same as saying that smaller initial particle size leads to smaller activation energy.

In our work we are using both materials with a 0.5 μm particle size which is higher that the particles studied by Matsui et al.

The accuracy of the estimated results is affected by the limitations of experimental arrangement used but the analysis of comparative results is valid. In this study, diffusion coefficient calculation was obtained considering the values as for the initial stage of sintering.

The observation of activation energy and diffusion coefficient shows that 3YTZ presents higher activation energy for the global sintering process in the initial stage and also a higher activation sintering for the diffusion mechanism. We proposed that this observation can be related with the grain growth observed in zirconia sintering. 8YSZ normally presents a faster grain growth than that in tetragonal zirconia [28]. The diffusion coefficient calculated also shows a higher coefficient for 8YSZ than the one for 3YTZ and these values also support the idea of a faster sintering and grain growth for 8YSZ.

Table 1 shows comparative experimental data and results from kinetics study.

3.2.3. Porosimetry

Pore volume and pore size distribution of the 10 min sintered samples at 1250 °C were determined.

Fig. 5 shows the pore volume vs. pore radius: the main pore size distribution is narrow for both samples. There are no pores larger than 0.1 μm. This fact indicates that a good particle packing was reached in the green compact prepared by slip casting. Both samples present similar initial conditions in porosity. The cubic zirconia shows a faster decrease in the pore volume and presents a smaller pore radius. This fact is in concordance with the activation energy. Smaller activation energy as 731 kJ/kmol for 8YSZ

and 887 for 3YTZ means a lower energy barrier to brake to initiate the sintering process. The faster reduction and the smaller pore size for this moment in sintering reflect and support this idea. A high reduction in open porosity was due to interparticle sintering and intense neck formation.

It can also be observed that the average pore volume is smaller for 8YSZ (0.039 μm) than the ones for 3YTZ (0.048 μm) in these conditions supporting the idea of a faster densification in the initial stage of sintering.

3.2.4. Microstructure

Fig. 6 shows the microstructure of compacts held at 1250 °C for 20 min. The figure shows the individual zirconia particles in the initial state of sintering showing the uniform distribution of pores in the particle packing. For a holding time of 20 min, a marked neck formation in the contact area between particles is observed. There is no important variation from 3YTZ to 8YSZ in the distribution and pores size.

The microstructure in Fig. 6 confirmed the presence of lower residual porosity observed in the mercury porosimetry with pores located between dense particles. Therefore, the high reduction in pore volume accompanied by a slight reduction in pore size was attributed to the gradual
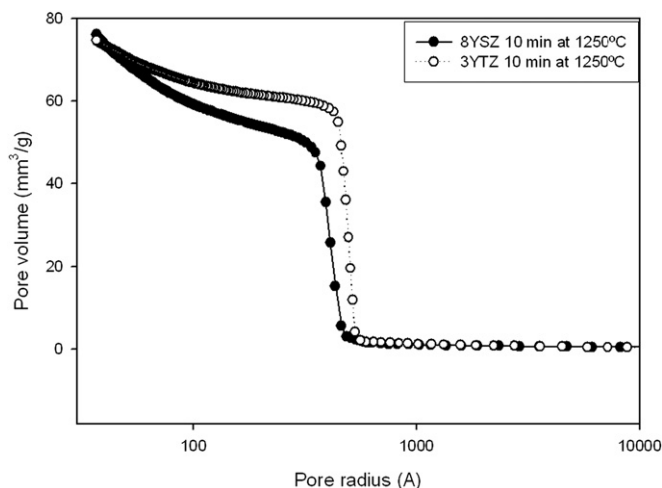

Fig. 5. Cumulative pore size distribution curves of samples sintered at 1250 °C for times of 10 min sintered.

Table 1
Summary of comparative sintering parameters measurements between 3YTZ and 8YSZ.

| Measurements	3YTZ	8YSZ
Initial particle size (d_{50}) (μm)	0.60	0.53
Relative green density (%)	0.65	0.60
Densification d/d_0% at 1400 °C 50 min	0.93	0.92
Sintering mechanism (n)	0.20–0.30	0.17–0.25
Activation energy of initial stage sintering (kJ/mol)	887	731
Activation energy of diffusion process (kJ/mol)	255	202
Diffusion coefficient (GBD) at 1400 °C (cm²/s)	4.05×10^{-14}	6.00×10^{-11}
Open pore size at 1250 °C 10 min (μm)	0.048	0.039
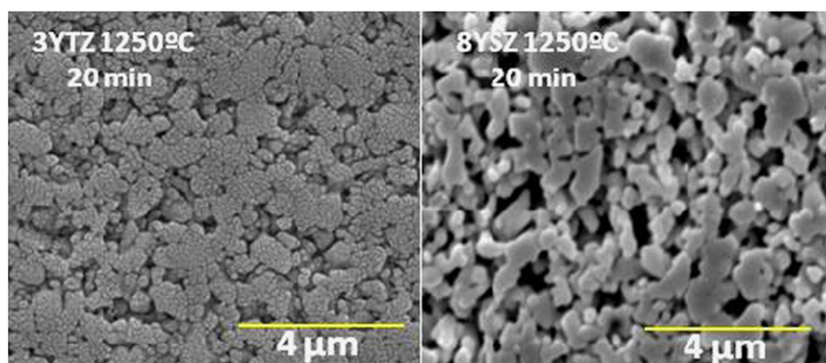
Fig. 6. SEM micrographs showing the microstructure of 3Y and 8Y tetragonal and cubic zirconia compacts sintered at 1250 °C for 20 min.

densification produced from the extensive formation of necks between particles. In this sintering stage, grain growth was not present as shown in this figure. The measurements of grain size confirmed this observation.

4. Conclusion

Isothermal sintering kinetic of zirconia with 3 and 8 mol% of yttria (3YTZ and 8YSZ) in tetragonal and cubic phase at isothermal condition was studied. Slip cast samples were sintered at temperatures between 1200 and 1450 °C for different soaking times. Sintering process evolution was followed by density, porosity measurements, and SEM microstructure observation.

As expected, the maximum density attainable increased with increasing sintering temperature, and high densification occurred at shorter times.

The sintering mechanism was estimated from the model proposed and both samples present a grain boundary diffusion mechanism which satisfactorily described the initial sintering process. From experimental data, the sintering activation energy for the global sintering process was calculated in 887 and 731 kJmol^{-1}, for 3YTZ and 8YSZ respectively. The Zr cation diffusion for grain boundary activation energy was also calculated by using the proposed model obtaining 255 and 202 kJmol^{-1} for 3YTZ and 8YSZ. The diffusion coefficients at 1400 °C were calculated for both materials as 4.05×10^{-14} cm^2 s^{-1} for 3YTZ and 6.00×10^{-11} cm^2 s^{-1} for 8YSZ.

Following these results supported by porosimetry measurements and SEM micrographs it is concluded that yttria content is favorable for sinterability in this range of concentration.

The values of diffusion coefficient show a greater diffusion coefficient for 8YSZ than that for 3YTZ at a fixed temperature. In this work it is proposed that the diffusion coefficient of Zr cations is also directly related to grain growth. The higher the diffusion coefficient, the faster the grain growth.

References

[1] R.C. Garvie., R.H. Hannink, R.T. Pascoe, Ceramic steel? Nature 258 (1975) 703–704.

[2] H. Zender, H. Leistner, H.R. Searle, ZrO materials for application in the ceramic industry?, Interceramic 39 (1990) 33–36.

[3] X. Guo, Can we achieve significantly higher ionic conductivity in nanostructured zirconia?, Scripta Materialia 65 (2011) 96–101.

[4] M. Hisbergues, S. Vendeville, P. Vendeville, Review zirconia: established facts and perspectives for a biomaterial in dental implantology, Journal of Biomedical Materials Research—Part B: Applied Biomaterials 88 (2009) 519–529.

[5] G. Maizza, S. Grasso, Y. Sakka, T. Noda, O. Ohashi, Relation between microstructure, properties and spark plasma sintering (SPS) parameters of pure ultrafine WC powder, Science and Technology of Advanced Materials 8 (2007) 644–654.

[6] R. Orru, R. Licheri, A.M. Locci, A. Cincotti, G. Cao, Consolidation/synthesis of materials by electric current activated/assisted sintering, Materials Science and Engineering: R: Reports 63 (2009) 127–287.

[7] M. Cologna, R. Raj, Surface diffusion controlled neck growth kinetics in early stage sintering of zirconia, with and without applied dc electric field, Journal of the American Ceramic Society 94 (2010) 391–395.

[8] M. Cologna, B. Rashkova, R. Raj., Flash sintering of nanograin zirconia in < 5 s at 850 °C, Journal of the American Ceramic Society 93 (2010) 3556–3559.

[9] I.W. Chen, X.H. Wang, Sintering dense nanocrystalline ceramics without final-stage grain growth, Nature 404 (2000) 168–171.

[10] A. Ghosh, A.K. Suri, B.T. Rao, T.R. Ramamohan, Low-temperature sintering and mechanical property evaluation of nanocrystalline 8 mol% yttria fully stabilized zirconia, Journal of the American Ceramic Society 90 (2007) 2015–2023.

[11] D.S. Kim, J.H. Lee, R.J. Sung, S.W. Kim, H.S. Kim, J.S. Park, Improvement of translucency in Al$_2$O$_3$ ceramics by two-step sintering technique, Journal of the European Ceramic Society 27 (2007) 3629–3632.

[12] C. Laberty-Robert, F. Ansart, C. Deloget, M. Gaudon, A. Rousset, Dense yttria stabilized zirconia: sintering and microstructure, Ceramics International 29 (2003) 151–158.

[13] S.Y. Lee, Sintering behavior and mechanical properties of injection-molded zirconia powder, Ceramics International 30 (2004) 579–584.

[14] F. Guo, A. Javed, I.P. Shapiro, P. Xiao, Effect of HCl concentration on the sintering behavior of 8 mol% Y$_2$O$_3$ stabilized ZrO$_2$ deposits produced by electrophoretic deposition (EPD), Journal of the European Ceramic Society 32 (2012) 211–218.

[15] J. Laurencin, G. Delette, F. Usseglio-Viretta, S.Di Iorio, Creep behaviour of porous SOFC electrodes: measurement and application to Ni-8YSZ cermets, Journal of the European Ceramic Society 31 (2011) 1741–1752.

[16] D.J. Chen, M.J. Mayo, Rapid rate sintering of nanocrystalline ZrO_2-3 mol% Y_2O_3, Journal of the American Ceramic Society 79 (1996) 906–912.

[17] R.L. Coble, Initial sintering of alumina and hematite, Journal of the American Ceramic Society 41 (1958) 55–62.

[18] W.H. Rhodes, R.E. Carter, Cationic self-diffusion in calcia-stabilized zirconia, Journal of the American Ceramic Society 49 (1966) 244–249.

[19] W.D. Kingery, M. Berg, Study of the initial stages of sintering solids by viscous flow, evaporation–condensation, and self-diffusion, Journal of Applied Physics 26 (1955) 1205–1212.

[20] R.C. Garvie, P.S. Nicholson, Phase analysis in zirconia systems, Journal of the American Ceramic Society 55 (1972) 303–305.

[21] G. Suárez, M.P. Albano, L.B. Garrido, E.F. Aglietti, Dispersion of concentrated aqueous yttria-stabilized zirconia with ammonium polyacrylate, Ceramics International 33 (2007) 925–929.

[22] G. Suárez, L.B. Garrido, E.F. Aglietti, Sintering kinetics of 8Y-cubic zirconia: cation diffusion coefficient, Materials Chemistry and Physics 110 (2008) 370–375.

[23] K. Matsui, A. Matsumoto, M. Uehara, N. Enomoto, J. Hojo, Sintering kinetics at isothermal shrinkage: effect of specific surface area on the initial sintering stage of fine zirconia powder, Journal of the American Ceramic Society 90 (2007) 44–49.

[24] K. Matsui, N. Ohmichi, M. Ohgai, T. Yamakawa, M. Uehara, N. Enomoto, J. Hojo, Initial sintering mechanism of fine zirconia particles including a small amount of alumina, Journal of the Ceramic Society of Japan 112 (2004) 343–349.

[25] K. Matsui, K. Tanaka, T. Yamakawa, M. Uehara, N. Enomoto, J. Hojo, Sintering kinetics at isothermal shrinkage: II, effect of Y_2O_3 concentration on the initial sintering stage of fine zirconia powder, Journal of the American Ceramic Society 90 (2007) 443–447.

[26] G. Suárez, Y. Sakka, Effect of alumina addition on initial sintering of cubic ZrO_2 (8YSZ), Ceramics International 36 (2009) 879–885.

[27] J. Wang, R. Raj, Estimate of the activation energies for boundary diffusion from rate-controlled sintering of pure alumina, and alumina doped with zirconia or titania, Journal of the American Ceramic Society 73 (1990) 1172–1175.

[28] R. Chaim, Activation energy and grain growth in nanocrystalline Y-TZP ceramics, Materials Science and Engineering A 486 (2008) 439–446.

[29] D.Sotiropoulou, P. Nikolopoulos, Surface and grain-boundary energies of cubic zirconia, Journal of Materials Science 26 (1991) 1395–1400.